TITLE: Lifetime of phosphorescence from nanoparticles yields accurate measurement of concentration of oxygen in microdroplets and allows to monitor the metabolism of bacteria.

AUTHOR NAMES: Michał Horka[1‡], Shiwen Sun[2‡], Artur Ruszczak[1], Piotr Garstecki[1*], and Torsten Mayr[2*]

AUTHOR ADDRESS:

1 Institute of Physical Chemistry, Polish Academy of Sciences, Kasprzaka 44/52, 01-224 Warsaw, POLAND

2 Institute of Analytical Chemistry and Food Chemistry, Graz University of Technology, Stremayrgasse9/2, 8010 Graz, AUSTRIA

ABSTRACT:

A method to monitor the level of oxygen in microdroplets is presented. Optical sensor nanoparticles are dispersed in the aqueous phase of the microfluidic droplets for culturing bacteria. The oxygen sensor nanoparticles consist of phosphorescent indicator dye embedded in poly(styrene-*block*-vinylpyrrolidone) nanobeads. The nanoparticles are excitable by red light and emit in the near-infrared spectra region which minimizes background fluorescence from biological matter. The biocompatibility of the nanoparticles was proven. Nanoparticles sensors were read out by adapted miniaturized oxygen meters. The instruments can be easily integrated into the microfluidic system by placing it next to the tubing and measuring through the tubing wall. The phosphorescence lifetime-based measurement circumvents the drawbacks of intensity-based measurements and enables the determination of the absolute oxygen concentration in individual moving droplets. The technique can also be used for monitoring the growth of bacteria in microdroplets. We demonstrate simultaneous measurement of concentration of oxygen and optical density (OD) from micro cultures of *E.coli* and *M.smegmatis*.

INTRODUCTION

Droplet microfluidic technologies allow to encapsulate, isolate and culture small groups of microorganisms[1,2]. The limited (nl to μl) volume of the reactor provides for the so called "stochastic confinement"[3] and effective concentration to measurable levels of metabolic products and secreted molecules. Compared with bulk cultures, culturing bacteria in droplet microfluidic systems is cost-effective as it uses small quantities of reagents, and can be used in high-throughput studies[4,5] because it is straightforward to generate and handle multiple droplet bioreactors. These features make up for an attractive platform for research in microbiology, including analysis of bacterial growth and adaptation in microdroplet chemostats[6], analyzing and sorting bacterial phenotypic diversity and high-throughput directed evolution of bacteria[7,8].

Both diagnostic procedures and research protocols often require the information about the growth rate of microbes. The most commonly used detection methods to characterize and monitor bacterial growth in microfluidic systems are i) detection of fluorescence, *i.e.* fluorescent proteins synthesized by bacteria[9–12] or fluorescent markers[13–15] ii) measurement of changes in optical density of the suspension caused by growth of bacteria[6,16,17], iii) monitoring bacterial enzymatic activity[18–21] or production rate of metabolic products, *i.e.* ethanol[22,23]. It is highly desirable to monitor the concentration of analytes which directly influence bacterial growth, for example concentration of oxygen. Oxygen uptake rate is one of the fundamental physiological parameters of the culture conditions[24]. A recent tutorial review summarized both electrochemical and optical approaches for implementing analysis on concentration of oxygen in microfluidic cell and tissue culture systems[25].

Monitoring oxygen concentration is of vital importance for growth and metabolism of aerobic bacteria in droplet bioreactor, since oxygen concentration could be an important constraint in the limited volume of droplets[26]. An accurate and reliable method for oxygen measurement in droplets could provide an important tool for the use of droplet microfluidic technologies in microbiology. Measurement of concentration of oxygen in droplets, however, presents several challenges: 1) requirement for high sensitivity of sensor and adequate intensity of signal due to the typically small (nl - μl) volume of droplets; 2) preference for miniaturized sensors and detectors that could be easily integrated with a microfluidic chip or a segment of tubing; 3) necessity for the sensor to be biocompatible and inert without any significant influence on the biological processes undergoing in droplets. Within the range of known methods of measurement of concentration of oxygen[27], optical oxygen sensing strategies seem to best comply with the requirements listed above. Optical sensors are highly sensitive with short response time, inert, compatible with miniature volumes and cost-effective.

While there are multiple examples of using optical oxygen sensor in single phase microfluidic systems for monitoring enzymatic reactions[28] and cell culturing conditions[29–32], and investigation of oxygen transfer[33,34],

the reports on measuring oxygen content in droplets are few. The most commonly used format of sensors for microfluidic applications is compatible with the planar structure of the chips: for example by gluing sensor foil or spraying sensor layer into the microfluidic channels. Droplet microfluidic applications require a different approach - the sensitive element must be in direct contact with the droplet (in biological applications – aqueous phase). Therefore, directly dissolving indicator or dispersing sensor nanoparticles are preferred formats. Abbyad *et al.* introduced oxygen sensitive dye into the aqueous phase[35]. They measured concentration of oxygen in droplets and showed that droplets can be oxygenated or deoxygenated by being carried by air-saturated or oxygen-free oil, respectively. Still, oxygen concentration was not monitored when red blood cells were introduced into the drops. Cao *et al.*[36] stained oxygen sensitive dye into polystyrene nanobeads and mixed oxygen-sensitive nanobeads with cell suspension. The authors used measurement of intensity of fluorescence to monitor concentration of oxygen in droplets during bacterial cultivation. And they retrieved only the relative change of oxygen concentration (i.e. fraction of oxygen consumed during incubation). The accuracy and precision of an intensity-based measurement suffers from uneven distribution of the dye in droplets or the geometry of the droplets, photo bleaching, and variations of the instrument. In a similar approach, Mahler *et al.*[26] dispersed oxygen-sensitive nanoparticles in cell culturing media and used lifetime-based measurement. They monitored only concentration of oxygen in a group of pl volume droplets trapped in a 3D printed micro-incubator.

Here we present a solution that offers on-line, real-time, and accurate measurement of concentration of oxygen in individual droplets in a microfluidic culturing system. We use optical oxygen sensitive nanoparticles in combination with phosphorescence lifetime-based measurement enabling the determination of absolute concentration of oxygen. We compare optical density (OD) and oxygen level in droplets during cultivation of *E.coli* and *M. smegmatis*. We also investigate oxygen transfer rate (OTR) from carrier oil phase to droplets and through tubing wall of microfluidic cell culturing system.

RESULTS AND DISCUSSION

Tubing-based microfluidic cell culturing device

We fabricated the microfluidic device using Teflon Fluorinated Ethylene Propylene (FEP) tubing (ID = 0.8 mm, OD = 1.6 mm) and customized fluidic connectors (Figure1.c and Figure S8). These connectors provide convenient flexibility to the tubing-based microfluidic system. Together with automation system, we are able to use tubings and connectors to build various functional modules, *e.g.* a module for fusion of two droplets with different contents, a module for splitting droplets into two parts and a module for sorting droplets. In this work, the microfluidic cell culturing system consists of two parts: a module for generation of droplets and another one for incubation of the colonies (Figure 1.a). The module for generation of

droplets comprises a T-junction. A three-way Teflon connector allows us to introduce the aqueous phase into the hydraulic line that carries the continuous liquid (oil). We generate aqueous droplets of desired volume by controlling the interval over which the aqueous phase is injected into the T-junction module. The average volume of droplets in this work is 4 µl. And we fix the rate of flow of the continuous liquid to 20 ml/h. Once formed, the droplets flow into the module for incubation. In this module, we place fibers on opposite sides of tubing for measurement of OD, and attach the Piccolo2 detector to the wall of the tubing for measurement of concentration of oxygen. We measure and record information of OD and concentration of oxygen in each droplet when they pass through the detection unit (Figure 1.b). We control the flow of droplets through the system with a set of external valves connected to pressurized reservoirs of oil and to outlets maintained at ambient (atmospheric) pressure. We use a custom written Lab View script to control all valves. This highly automated system enables precise handling of droplets for bacterial culturing[6,37].

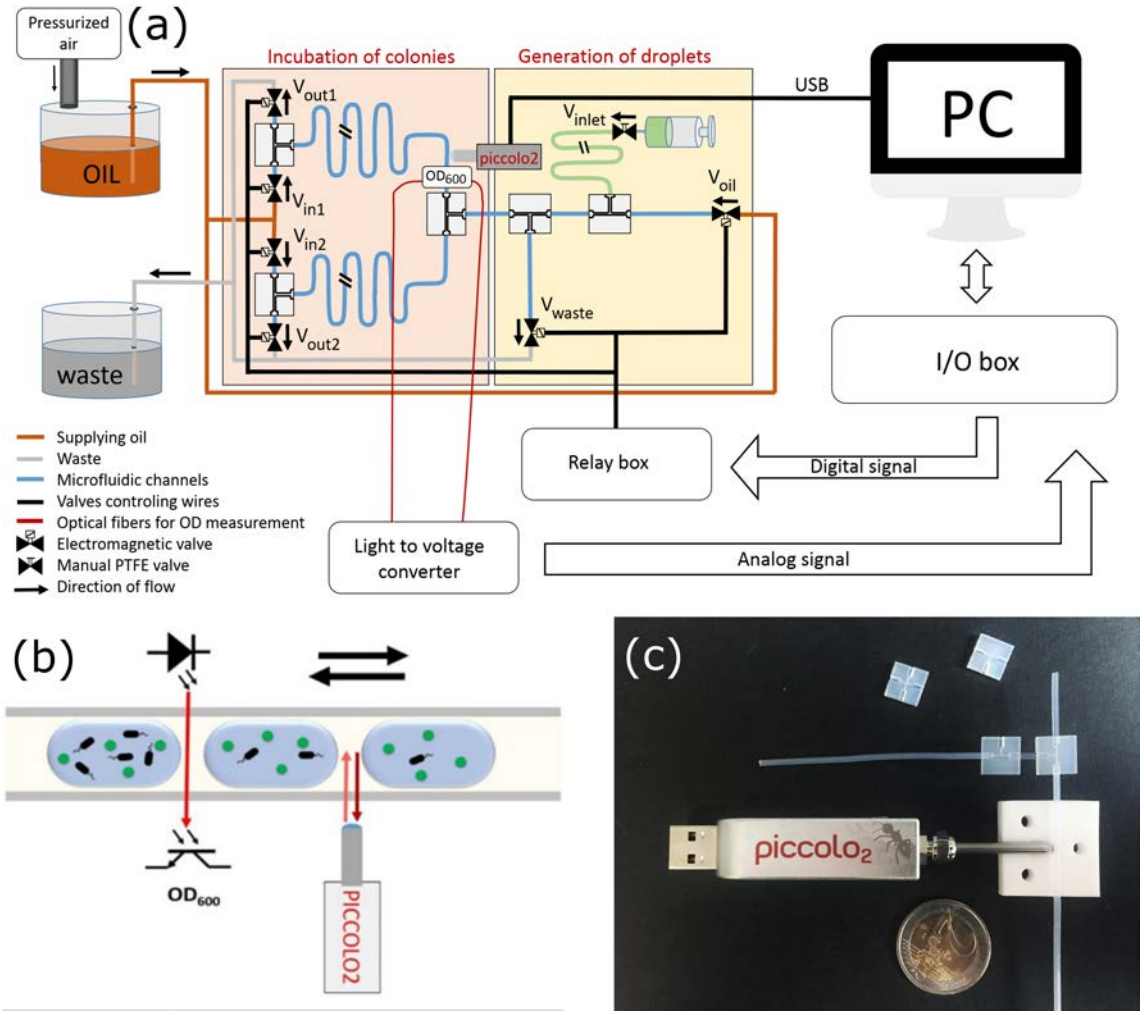

Figure 1. (a) Scheme of microfluidic cell culturing system including two parts: generation of droplets and incubation of colonies; (b) zoom-in of detection unit in the incubation part including measurements for Optical Density (OD) and concentration of oxygen in droplets; (c) picture of tubings connected by customized fluidic connectors and with Piccolo2 placed next to it and fixed by a homemade holder (only bottom part is shown).

Compatibility of oxygen sensor nanoparticles and microfluidic cell culturing system

Oxygen sensor nanoparticles are made by entrapping oxygen indicator dye Platinum(II) *meso*-tetra(4-fluorophenyl)tetrabenzoporphyrin (PtTPTBPF) in poly(styrene-*block*-vinylpyrrolidone) (PSPVP) nanobeads. The indicator PtTPTBPF is excited by red light and emits in near-infrared wavelengths (above 700 nm). This range of frequencies is particularly compatible with measurements on biological systems because it minimizes background fluorescence and has little interference with cells[38]. Additionally, other optical channels, *i.e.* channels for autofluorescence or fluorescent protein/ markers, are still available for simultaneous measurements. The core-shell structure of the PSPVP nanobeads makes it possible to disperse the beads in aqueous phase and to immobilize oxygen indicator in the lipophilic core formed by nonpolar polystyrene blocks[39,40]. Furthermore, using nanoparticles with sensing dye entrapped shows the great advantages over directly dissolving indicator dye in droplets. The nanoparticle structure shields the sensor molecules and prevents any interferences from the sample *i.e.* proteins. Nevertheless, many of the indicators possess extreme low solubility in aqueous solutions. Also sensor nanoparticles exhibit short response time, no dye leaching, and long storage period[41], which are ideal for microfluidic applications. The nanoparticles have an average diameter of 180 ± 5 nm, together with TEM images reported by *Ehgartner et al.*[28].The spectral properties of this oxygen sensor nanoparticles are compatible with the miniaturized, commercially available, phosphorescence lifetime-based read-out instrument Piccolo2 (Figure 1.c) equipped with a focusing lens, as reported recently[42]. The Piccolo2 can measure through the wall of a tubing (or other transparent materials *e.g.* polycarbonate, polystyrene, PDMS, and glass) at any location of the microfluidic system. By using lifetime-based measurement, instead of intensity-based measurements, we are able to accurately characterize oxygen concentration in microdroplets. The lifetime is an intrinsic property of oxygen sensor nanoparticles and is not affected by instrument variations, sample turbidity, or ambient environment. Details of optical oxygen sensing principle and full calibration curves of the oxygen sensor nanoparticles at room temperature (20 °C) and incubation temperature (37 °C) are available in the supporting information.

To check that the oxygen sensor nanoparticles are not affected by the procedures used to treat the growth media for bacteria, we compared the calibration curves of the sensor nanoparticles before and after five cycles of autoclave procedure (121 °C for 15 minutes). We have not seen any significant change in the sensitivity of the nanoparticles to concentration of oxygen (Figure S2). Besides, the sensor nanoparticles show effects on the growth of neither Gram positive (*S.epidermidis*) nor Gram negative (*E.coli*) strains. We check the survival rate of both *S.epidermidis* and *E.coli* with different dilution factors of sensor nanoparticles suspension (Figure S3.a). We also obtain same growth curves of *E.coli* with and without oxygen sensor nanoparticles present in LB media (Figure S3.b).

On-line real-time measurements of concentration of oxygen in microdroplets

First of all, we demonstrate that the oxygen sensor nanoparticles yield an accurate and reliable measurement of concentration of oxygen in the following settings: i) in a bulk solution, ii) in continuous flow in a tubing and iii) in microdroplets flowing in a tubing (see Table 1). We prepared both oxygen free and air saturated aqueous solutions with suspended oxygen sensor nanoparticles. We then measured the phase shift angle and calculated lifetime for oxygen free condition (τ_0) and lifetime for air saturated condition (τ). The ratio of τ_0 and τ defines the calibration curve for a given batch of sensor nanoparticles. The difference of this ratio is negligible between the measurements from continuous (single phase) flow and from microdroplets in the tubing, which shows the feasibility of using oxygen sensor nanoparticles for measurements of concentration of oxygen inside microdroplets. The resolution of this oxygen sensor nanoparticles for low oxygen range (50 µM) and high oxygen range (air-saturation) are 0.07 µM and 0.12 µM, respectively (1 atm, 20 °C).

Table 1. Comparison of signal (phase shift) recorded from oxygen sensor nanoparticles and calculated lifetime (τ) from the same solutions at oxygen free and air saturated conditions of settings i) in a bulk solution, ii) in continuous flow in a tubing, and iii) in microdroplets flowing in a tubing.

Dimensions	oxygen free		air saturated		τ_0/τ
	phase shift / °	τ_0 / µs	phase shift / °	τ / µs	
bulk	55.68±0.01	58.29±0.02	23.77±0.01	17.52±0.01	3.33
continuous flow	55.18±0.07	57.21±0.15	23.88±0.02	17.62±0.02	3.25
microdroplets	55.15±0.03	57.15±0.06	23.87±0.04	17.61±0.03	3.25

We carry out the measurement of concentration of oxygen in microdroplets at a frequency of 10 Hz (the sampling frequency is limited by electronics of Piccolo2). When each droplet passes through detection unit, we are able to acquire 7 – 8 measurements on each of the droplets. Our acquisition system records both the phase shift angle and the intensity of phosphorescence from the nanoparticles (Figure 2.a).

The quality of the signal recorded from the droplet depends on the particular part of the drop that is illuminated. The droplets are confined by the walls of the tubing and in the first approximation they acquire the shape of cylinders truncated with hemi-spherical caps. When the excitation light passes through the cylindrical body of the droplet, which is the longest optical path, we detect high intensity of signal from phosphorescent nanoparticles. In contrast, we detect low intensity of signal when measuring on the cap of the droplet. Similarly, when measuring at continuous liquid (oil), which contains no nanoparticles, the signal intensity is negligible. We use the intensity of the signal as a parameter to select the measuring window for reading the phase shift angle, *i.e.* the signal that provides reliable information on oxygen concentration inside the droplets. The average value of phase shift angle is then used to calculate lifetime of phosphorescent nanoparticles and to determine concentration of oxygen in the droplets. Interestingly,

while the signal intensity is prone to variation, coming from the geometry of the droplet, the synchronization of the measurement to the passage of the droplet *etc.*, the phase shift angles of droplets at same level of oxygen are the same in each of the droplets with non-identical content of nanoparticles (different in signal intensity). Once again, it shows the advantages of using lifetime-based measurement over intensity-based measurement.

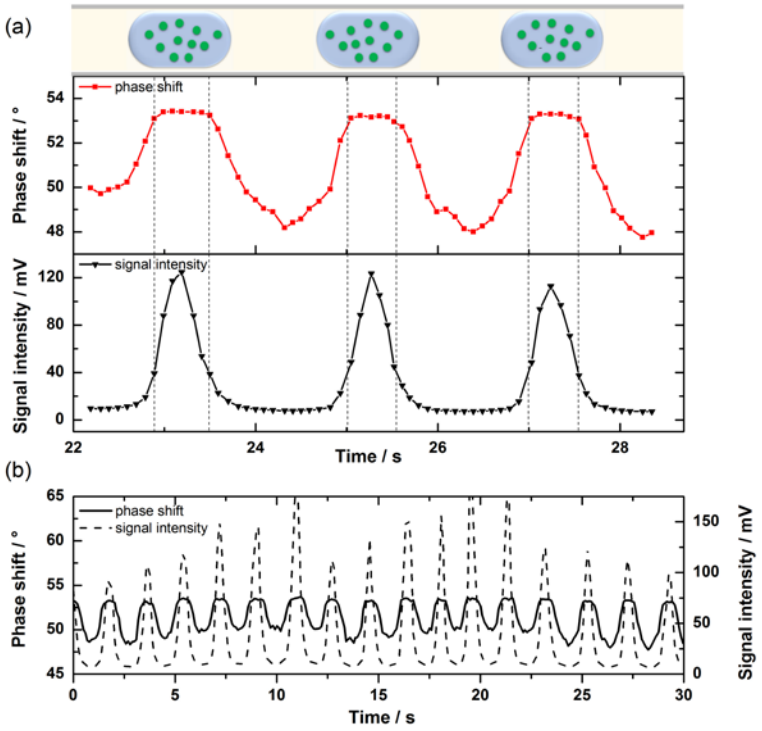

Figure 2. (a) Illustration of corresponding phase shift angle and signal intensity recorded when measuring at different positions of droplets or oil. High signal intensity indicates measuring in cylindrical body of the droplet. Low signal intensity indicates measuring at caps of the droplet. When measuring at oil, there is negligible signal intensity. (b) Example of online sensing data of a train of droplets. Phase shift angle is recorded into log only when signal intensity is above 40 mV. The average value of phase shift angle of this train of droplets is 53.27 ± 0.18 degree.

Monitoring bacterial growth and concentration of oxygen in microdroplets

We grow two species of bacteria, *Escherichia coli* ATCC 35218 and *Mycobacterium smegmatis PCM 661 (Polish Collection of Microorganisms)* in microdroplets. In each experiment, we generate 10 identical droplets. We seed bacteria in the mixture of fresh media (LB medium for *E. coli* and Middlebrook medium enriched with Middlebrook OADC for *M. smegmatis*) and oxygen sensor nanoparticles. In addition we also formed control sets of droplets that contained only the fresh media and oxygen sensor nanoparticles. In the experiment we cycle the droplets back and forth in the incubation part of the system. Every 10 minutes, we record both OD at λ = 600 nm and oxygen concentration from each droplet to obtain the evolution of concentration of oxygen and optical density (Figure 3 and Figure 4). We calculate the mean values of OD and oxygen concentration for the ten droplets in each set. The error bars represent the standard derivation

of this mean. The OD measurements show a typical exponential growth curve of *E.coli* in microdroplets, while, in the control set, OD remains at almost zero level. This indicates that we do not have cross-contamination (*i.e.* transfer) of bacterial cells between the droplets during incubation.

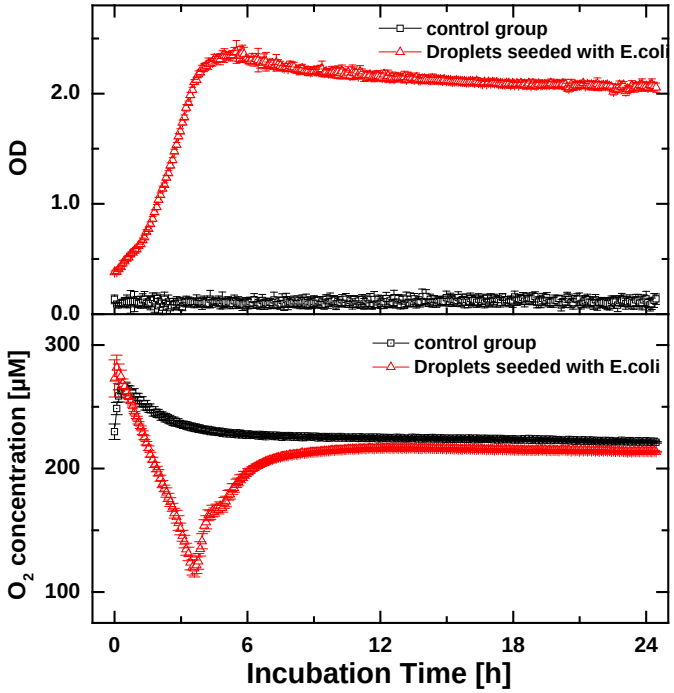

Figure 3. Monitoring of OD (Top) and concentration of oxygen (Bottom) during 24 hours incubation of control set of droplets and experiment set - droplets seeded with *E.coli* ATCC35218.

In both sets, the evolution of oxygen concentration shows a small hump at the very beginning of incubation. This small increase of oxygen concentration in droplets is due to two reasons: i) continuous liquid (FC40) has a higher solubility of oxygen than the aqueous phase. There is a non-negligible mass transfer of oxygen from oil to droplets. We observed fast transfer of oxygen from air-saturated oil to a single deoxygenated droplet when flowing in the tubing (Figure S4). ii) The droplets are generated at room temperature (20 °C), and only later transferred to the incubation part of the system that is maintained at a higher temperature (37 °C). The calibration curves show that the phase-shift recorded from the oxygen sensor nanoparticles is sensitive to temperature. So before the droplets reach the incubation temperature, there is a small difference of measured and real oxygen concentration in droplets.

The most significant effect that we observe is the decrease of oxygen concentration in the droplets containing *E.coli*. We observe a simultaneous increase of OD in these droplets, reflecting the first, exponential phase of growth of the colony of microbes. This is consistent with that in the exponential growing phase, *E.coli* has the greatest oxygen consumption rate. This huge amount of oxygen consumed in the exponential growth phase leads to the substantial decrease of oxygen concentration in the droplets. We do not observe this phenomenon in the control group.

Eventually, the concentration of oxygen in the droplets reaches an equilibrium level. From the growth curve of *E.coli* in droplets, we can see the bacteria are at the stationary phase, characterized by a limited oxygen consumption rate. The fluorinated oil provides sufficient oxygen supply to the droplets which compensates the oxygen consumed by bacteria in the droplets. The transfer of oxygen from oil into the aqueous phase is a rather fast process. We show that a single oxygen-free droplet needs around 15 seconds to reach air-saturation after immersion in air-saturated oil (FC40) in our microfluidic system (Figure S4). The fluorinated oil (FC40) has a much higher oxygen solubility than water. And in this droplet microfluidic culturing system, the volume of continuous phase (oil) is hundreds times of the volume of droplets in the system. Nevertheless, the Teflon FEP tubing shows good oxygen permeability (Figure S6). So we haven't observed complete oxygen depletion in our study. The stable value of oxygen concentration in droplets are similar in both experimental and control group droplets.

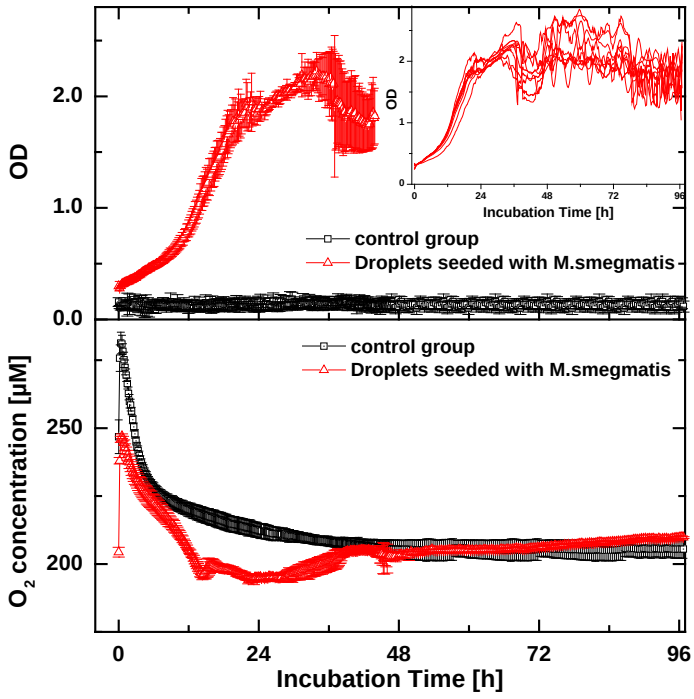

Figure 4. Monitoring of OD (top) and concentration of oxygen (bottom) during 96 hours incubation of control set of droplets and droplets seeded with *M.smegmatis* PCM661; inset: OD measurement of each of 10 droplets seeded with *M.smegmatis* during 96 hours incubation.

We also performed an analogous set of experiments to the ones described above but with *M.smegmatis*. *M.smegmatis* comes from the same genus (*Mycobacterium*) as a pathogenic factor for tuberculosis (*Mycobacterium tuberculosis*). M.smegmatis grows slowly (a doubling time of 3 to 4 hours) and has an tendency to clump[43]. The clumps cause fluctuation in the OD measurement. We added Tween 20 in the growth media to reduce clumping, but the OD measurement still shows substantially higher error bars for each measurement (Figure 4 and the inset) than in the case of *E.coli*. Meanwhile, monitoring of the oxygen

concentration is not influenced by clumping of *M. smegmatis*. The relative standard deviation of each measurement point is comparable to the experiment with *e. coli* (Figure 3). The oxygen concentrations is decreased during exponential growing phase, but it remains at a high level. On one hand, the long doubling time gives small rate of oxygen consumption by *M.smegmatis*. On the other hand, the oil phase supplies oxygen into droplets during incubation. We still detect a slight difference of oxygen concentration between the experimental set and the negative control set. The oxygen sensor nanoparticles provide a feasible method for measuring the concentration of oxygen also in cultures of bacteria that aggregate. This potentially can be adapted to detect growth of slow growing bacteria by monitoring oxygen uptake.

CONCLUSIONS

We have shown accurate online phosphorescence lifetime-based measurement of dissolved oxygen inside of microdroplets using oxygen sensor nanoparticles. These sensor nanoparticles show great potential for biological applications in microfluidic systems since they are autoclavable, not interfering with microorganism, easy to integrate with microfluidic devices.

We demonstrated simultaneous monitoring of both the concentration of oxygen and OD in droplets during incubation of *E.coli* and *M.smegmatis*. It is the first time we reveal the profile of absolute values of oxygen concentration in each droplets during bacterial incubation. The oxygen sensor nanoparticles are robust in non-perfect suspensions, *i.e.* clumping cell culture. The accurate characterization of dissolved oxygen will be useful in engineering of oxygen supply in the microenvironment for bacterial growth in droplet microfluidic culturing systems.

Other applications of droplet microfluidic technologies could also benefit from accurate characterization of oxygen concentration in droplets with this simple tactic of measuring oxygen concentration in small volumes. The system certainly allows for fundamental studies of oxygen transfer and mass transfer in microfluidic systems.

MATERIALS AND METHODS

Preparation of oxygen sensor nanoparticles and calibration

Oxygen sensor nanoparticles were prepared by staining oxygen sensitive dye Platinum(II) *meso*-tetra(4-fluorophenyl)tetrabenzoporphyrin (PtTPTBPF) in poly(styrene-*block*-vinylpyrrolidone) (PSPVP) beads. The oxygen sensitive dye PtTPTBPF was synthesized in-house, and has absorption maximum at 430 nm and 614 nm, and emission wavelength at 760 nm[38]. The preparation of sensor nanoparticles was following the procedure reported by Borisov *et al.*[41]. Briefly, PSPVP polymer emulsion is diluted with the mixture of ethanol and water. PtTPTBPF is dissolved in ethanol and added dropwise into polymer emulsion. Then we

concentrated the emulsion under reduced pressure until all ethanol is removed. The oxygen sensor nanoparticles were calibrated at both 20 °C and 37 °C (see Figure S1).

Frequency-domain lifetime measurement (phase shift) was conducted by Fiber-Optic Oxygen Meter Piccolo2 (Pyro Science GmbH, Germany) equipped with focusing lens (GRINTECH GmbH, Germany) which enables detection in microfluidic channels. The excitation light is focused to an area about 80 µm inside the channel[42]. Measuring frequency used in this work is 10 Hz.

This method has an intensity-modulated light as excitation source. The time lag between absorption and emission causes the delay of emission light to modulated excitation light. This delay is recorded as angle of phase shift (φ). The relation between phase shift angle and lifetime of oxygen sensitive probe is described below[44]:

$$\tau = \frac{\tan \varphi}{2\pi f} \qquad \text{Eq. 1}$$

Where φ is phase shift angle (dphi); f is the frequency of modulation of light source.

Microfluidic cell culturing device

We fabricated similar system to Cybulski *et al.* work[37]. We built a single T-junction to generate droplets with the same content and incubating module to culture bacteria. Our system was extended by Piccolo2 reader to measure oxygen level in passing droplets. First, we use a syringe pump to fill up aspiration tube with aqueous solution. During this procedure the manual valve close to the syringe and valve V_{waste} are opened. Then we close the manual valve and remove the rest of solution by oil from valve V_{oil}. After pressure is stabilized in the tubing, the system is ready to generate droplets for incubation. To generate droplets, valve V_{inlet} is switched on while valve V_{waste} is opened to maintain constant hydrodynamic resistant in the system. After the generation, we flow the droplets into incubation part by switching valves V_{oil} and $V_{out1.}$ After the generation of a set number of droplets system moved automatically to incubation state. During this state we open the valves V_{in1}-V_{out2} and V_{in2}-V_{out1} alternatively to cycle the droplets back and forth.

In our system we have two independent readouts from each droplet: oxygen concentration *via* Piccolo2 and optical density *via* custom build electronic. We use the signal from Piccolo2 in feedback loop to count droplets. We measure OD at 600 nm with red LED and a light to voltage converter (TSL257, ams AG, formerly TAOS). Voltage signal is filtered and gained by custom made electronic and then acquired by National Instruments I/O device (SCB68). We collect samples with a frequency of 20kHz. For each droplet we measure mean value from 50% of samples from middle part of the droplet. The time needed for a droplet to pass under OD reader is around 700ms therefore the result for each droplet is calculated from around 7000 samples.

During the demonstration of oxygen measurement in droplets (Figure 2), we used two syringe pumps (World Precision Instruments, USA) to generate droplets *via* a T-junction built by fluidic connector.

Bacteria and Media used

We used two species of bacteria: fast growing *Escherichia coli* ATCC 35218, and slow growing *Mycobacterium smegmatis* PCM 661 (Polish Collection of Microorganisms). We cultivated *E. coli* in LB medium (Roth, Germany) with addition of 100 µg/ml ampicillin (Roth, Germany), and *M. smegmatis* in Middlebrook 7H9 (BD, New Jersey, USA) medium enriched with OADC enrichment (BD, New Jersey, USA), plus 1% Tween 80 (Sigma Aldrich, Germany) (in order to avoid clumping of bacterial cells).

For each experiments we used freshly seeded bacteria in final optical density 0.2, which we diluted with nanoparticles, reaching 20x diluted sensors.

SUPPORTING INFORMATION

Characterization of optical oxygen sensor nanoparticles and investigation of oxygen transfer in microdroplets cell culturing system.

AUTHOR INFORMATION

Corresponding Authors

T.M.: E-mail: torsten.mayr@tugraz.at. Tel: (+43) 316 873 32504

P.G.: E-mail: garst@ichf.edu.pl. Tel: (+48) 22 343 22 33

Author Contributions

‡M.H. and S.S. contributed equally.

ACKNOWLEDGEMENTS

This work has received funding from the People Programme (Marie Curie Actions, Multi-ITN) of the European Union's Seventh Framework Programme for research, technological development and demonstration under grant agreement no° 608104 (EUROMBR) and the European Research Council Starting Grant 279647. PG additionally acknowledges support from the Foundation for Polish Science with the Idee dla Polski programme.

REFERENCES

(1) Kaminski, T. S.; Scheler, O.; Garstecki, P. *Lab Chip* **2016**.
(2) Theberge, A. B.; Courtois, F.; Schaerli, Y.; Fischlechner, M.; Abell, C.; Hollfelder, F.; Huck, W. T. S. *Angew. Chem. Int. Ed.* **2010**, *49* (34), 5846–5868.
(3) Vincent, M. E.; Liu, W.; Haney, E. B.; Ismagilov, R. F. *Chem. Soc. Rev.* **2010**, *39* (3), 974.

(4) Guo, M. T.; Rotem, A.; Heyman, J. A.; Weitz, D. A. *Lab. Chip* **2012**, *12* (12), 2146.
(5) Kintses, B.; van Vliet, L. D.; Devenish, S. R.; Hollfelder, F. *Curr. Opin. Chem. Biol.* **2010**, *14* (5), 548–555.
(6) Jakiela, S.; Kaminski, T. S.; Cybulski, O.; Weibel, D. B.; Garstecki, P. *Angew. Chem. Int. Ed.* **2013**, *52* (34), 8908–8911.
(7) Baraban, L.; Bertholle, F.; Salverda, M. L. M.; Bremond, N.; Panizza, P.; Baudry, J.; de Visser, J. A. G. M.; Bibette, J. *Lab. Chip* **2011**, *11* (23), 4057.
(8) Boitard, L.; Cottinet, D.; Bremond, N.; Baudry, J.; Bibette, J. *Eng. Life Sci.* **2015**, *15* (3), 318–326.
(9) Huebner, A.; Srisa-Art, M.; Holt, D.; Abell, C.; Hollfelder, F.; deMello, A. J.; Edel, J. B. *Chem. Commun.* **2007**, No. 12, 1218.
(10) Martin, K.; Henkel, T.; Baier, V.; Grodrian, A.; Schön, T.; Roth, M.; Michael Köhler, J.; Metze, J. *Lab Chip* **2003**, *3* (3), 202–207.
(11) Bjork, S. M.; Sjostrom, S. L.; Andersson-Svahn, H.; Joensson, H. N. *Biomicrofluidics* **2015**, *9* (4), 44128.
(12) Shim, J.; Olguin, L. F.; Whyte, G.; Scott, D.; Babtie, A.; Abell, C.; Huck, W. T. S.; Hollfelder, F. *J. Am. Chem. Soc.* **2009**, *131* (42), 15251–15256.
(13) Courtois, F.; Olguin, L. F.; Whyte, G.; Theberge, A. B.; Huck, W. T. S.; Hollfelder, F.; Abell, C. *Anal. Chem.* **2009**, *81* (8), 3008–3016.
(14) Lyu, F.; Xu, M.; Cheng, Y.; Xie, J.; Rao, J.; Tang, S. K. Y. *Biomicrofluidics* **2015**, *9* (4), 44120.
(15) Scheler, O.; Kaminski, T. S.; Ruszczak, A.; Garstecki, P. *ACS Appl. Mater. Interfaces* **2016**, *8* (18), 11318–11325.
(16) Churski, K.; Kaminski, T. S.; Jakiela, S.; Kamysz, W.; Baranska-Rybak, W.; Weibel, D. B.; Garstecki, P. *Lab. Chip* **2012**, *12* (9), 1629.
(17) Zang, E.; Brandes, S.; Tovar, M.; Martin, K.; Mech, F.; Horbert, P.; Henkel, T.; Figge, M. T.; Roth, M. *Lab. Chip* **2013**, *13* (18), 3707.
(18) Huebner, A.; Olguin, L. F.; Bratton, D.; Whyte, G.; Huck, W. T. S.; de Mello, A. J.; Edel, J. B.; Abell, C.; Hollfelder, F. *Anal. Chem.* **2008**, *80* (10), 3890–3896.
(19) Baret, J.-C.; Miller, O. J.; Taly, V.; Ryckelynck, M.; El-Harrak, A.; Frenz, L.; Rick, C.; Samuels, M. L.; Hutchison, J. B.; Agresti, J. J.; Link, D. R.; Weitz, D. A.; Griffiths, A. D. *Lab. Chip* **2009**, *9* (13), 1850.
(20) Lim, J.; Vrignon, J.; Gruner, P.; Karamitros, C. S.; Konrad, M.; Baret, J.-C. *Appl. Phys. Lett.* **2013**, *103* (20), 203704.
(21) Najah, M.; Mayot, E.; Mahendra-Wijaya, I. P.; Griffiths, A. D.; Ladame, S.; Drevelle, A. *Anal. Chem.* **2013**, *85* (20), 9807–9814.
(22) Abalde-Cela, S.; Gould, A.; Liu, X.; Kazamia, E.; Smith, A. G.; Abell, C. *J. R. Soc. Interface* **2015**, *12* (106), 20150216–20150216.
(23) Churski, K.; Ruszczak, A.; Jakiela, S.; Garstecki, P. *Micromachines* **2015**, *6* (10), 1514–1525.
(24) Garcia-Ochoa, F.; Gomez, E.; Santos, V. E.; Merchuk, J. C. *Biochem. Eng. J.* **2010**, *49* (3), 289–307.
(25) Oomen, P. E.; Skolimowski, M. D.; Verpoorte, E. *Lab Chip* **2016**, *16* (18), 3394–3414.
(26) Mahler, L.; Tovar, M.; Weber, T.; Brandes, S.; Rudolph, M. M.; Ehgartner, J.; Mayr, T.; Figge, M. T.; Roth, M.; Zang, E. *RSC Adv* **2015**, *5* (123), 101871–101878.
(27) Wang, X.; Wolfbeis, O. S. *Chem. Soc. Rev.* **2014**, *43* (10), 3666.
(28) Ehgartner, J.; Strobl, M.; Bolivar, J. M.; Rabl, D.; Rothbauer, M.; Ertl, P.; Borisov, S. M.; Mayr, T. *Anal. Chem.* **2016**.
(29) Sud, D.; Mehta, G.; Mehta, K.; Linderman, J.; Takayama, S.; Mycek, M.-A. *J. Biomed. Opt.* **2006**, *11* (5), 50504.
(30) Mehta, G.; Mehta, K.; Sud, D.; Song, J. W.; Bersano-Begey, T.; Futai, N.; Heo, Y. S.; Mycek, M.-A.; Linderman, J. J.; Takayama, S. *Biomed. Microdevices* **2007**, *9* (2), 123–134.
(31) Lam, R. H. W.; Kim, M.-C.; Thorsen, T. *Anal. Chem.* **2009**, *81* (14), 5918–5924.
(32) Grist, S.; Schmok, J.; Liu, M.-C.; Chrostowski, L.; Cheung, K. *Sensors* **2015**, *15* (8), 20030–20052.
(33) Chen, J.; Kim, H. D.; Kim, K. C. *Microfluid. Nanofluidics* **2013**, *14* (3–4), 541–550.
(34) Ungerböck, B.; Pohar, A.; Mayr, T.; Plazl, I. *Microfluid. Nanofluidics* **2013**, *14* (3–4), 565–574.
(35) Abbyad, P.; Tharaux, P.-L.; Martin, J.-L.; Baroud, C. N.; Alexandrou, A. *Lab. Chip* **2010**, *10* (19), 2505.
(36) Cao, J.; Nagl, S.; Kothe, E.; Köhler, J. M. *Microchim. Acta* **2014**, 1–10.
(37) Cybulski, O.; Jakiela, S.; Garstecki, P. *Lab Chip* **2016**, *16* (12), 2198–2210.

(38) Borisov, S. M.; Nuss, G.; Haas, W.; Saf, R.; Schmuck, M.; Klimant, I. *J. Photochem. Photobiol. Chem.* **2009**, *201* (2–3), 128–135.
(39) Nagarajan, R.; Barry, M.; Ruckenstein, E. *Langmuir* **1986**, *2* (2), 210–215.
(40) Haulbrook, W. R.; Feerer, J. L.; Hatton, T. A.; Tester, J. W. *Environ. Sci. Technol.* **1993**, *27* (13), 2783–2788.
(41) Borisov, S. M.; Mayr, T.; Klimant, I. *Anal. Chem.* **2008**, *80* (3), 573–582.
(42) Ehgartner, J.; Sulzer, P.; Burger, T.; Kasjanow, A.; Bouwes, D.; Krühne, U.; Klimant, I.; Mayr, T. *Sens. Actuators B Chem.* **2016**, *228*, 748–757.
(43) Klann, A. G.; Belanger, A. E.; Abanes-De Mello, A.; Lee, J. Y.; Hatfull, G. F. *J. Bacteriol.* **1998**, *180* (1), 65–72.
(44) Holst, G. A.; Kuehl, M.; Klimant, I. V. Scheggi, A., Ed.; 1995; pp 387–398.

For TOC only